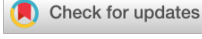
# RESEARCH ARTICLE



WILEY

# From wetlands to wetlandscapes: Remote sensing calibration of process-based hydrological models in heterogeneous landscapes

Connor Mullen 1 | Leonardo E. Bertassello 1 | P. Suresh C. Rao 2,3 0 | Marc F. Müller 1

#### Correspondence

Leonardo E. Bertassello, Department of Civil and Environmental Engineering and Earth Sciences, University of Notre Dame, Notre Dame, IN, USA.

Email: lbertass@nd.edu

#### **Funding information**

National Science Foundation, Grant/Award

Number: EAR 2142967

#### **Abstract**

Wetlands are vital components of landscapes that sustain a range of important ecosystem services. Understanding how wetland-rich landscapes-or wetlandscapeswill evolve under a changing climate and increasing anthropogenic encroachment is urgent. Wetlandscapes are highly heterogeneous, and scaling local modelling insights from individual instrumented wetlands to characterize landscape-scale dynamics has been a pervasive challenge. We investigate the potential to use water extent information from satellite imagery to calibrate landscape-scale process-based hydrological models. Applications to wetlandscapes in the Prairie Pothole Region (PPR) in North Dakota and the Texas Playa Lakes (TPL) shed light on two important trade-offs. First, in-situ monitoring provides accurate water extent information on an arbitrary subset of wetlands, whereas satellite imagery captures landscape-scale hydrological dynamics but suffers persistent water-detection challenges. Satellite imagery is a superior source of data for model calibration in sparsely monitored and spatially heterogeneous landscapes like the PPR, where the sampling uncertainty of monitored wetlands exceeds the water detection uncertainty of remote sensing. The two data sources are equivalent for more homogeneous landscapes like the TPL. The second tradeoff concerns the spatial resolution and temporal coverage of satellite imagery. In that regard, the 20 years of bi-weekly images captured by Landsat 7 provides unprecedented insights into the dynamic nature of the ecohydrological characteristics of wetlandscapes, such as seasonal and inter-annual changes of their metapopulation capacity. In the PPR, the amplitude of these dynamics far exceeds the bias introduced by Landsat's inability to capture ecologically important connectivity details due to its coarse spatial resolution compared to more recent imagery.

#### KEYWORDS

hydrologic regime, process-based hydrological model, remote sensing, wetlands

# 1 | INTRODUCTION

Wetlands are vital eco-hydrological components of landscapes. Their spatiotemporal dynamics affect several important ecosystem services (Keddy, 2010; LaBaugh, 1986), including flood protection (Acreman &

Holden, 2013), nutrients and carbon cycling (Cheng & Basu, 2017; Cronk & Fennessy, 2016), and they also serve as critical habitats to a wide range of unique flora and fauna (Dudgeon et al., 2006; Euliss et al., 2004). Wetlands can consist of a wide range of hydrologic features, from large permanent waters that provide important hydrologic

<sup>&</sup>lt;sup>1</sup>Department of Civil and Environmental Engineering and Earth Sciences, University of Notre Dame, Notre Dame, Indiana, USA

<sup>&</sup>lt;sup>2</sup>Lyles School of Civil Engineering, Purdue University, West Lafayette, Indiana, USA

<sup>&</sup>lt;sup>3</sup>Agronomy Department, Purdue University, West Lafayette, Indiana, USA

functions to smaller ephemeral ponds that provide important biogeochemical functions (Evenson et al., 2018). These features do not function in isolation but form a landscape mosaic (here referred to as wetlandscape) that sustains unique and fragile ecosystems (Brice et al., 2022; Dahl, 1990; Erwin, 2009; Van Meter & Basu, 2015; Walpole & Davidson, 2018). Ephemeral wetlands, in particular, account for approximately 60% of global wetlands (Papa et al., 2006) and are critically important in their ability to generate windows of transient connectivity for species dispersal and occupancy. Because wetlands often occur as discrete, heterogeneous patches distributed within a matrix of upland habitat (Leibowitz, 2003; Mushet et al., 2016), many species of wetland-dependent fauna exist as metapopulations that exchange individuals among patches through dispersal (Gibbs, 2000). Local populations of wetland species are often small and isolated (Semlitsch & Bodie, 1998). They are therefore vulnerable to spatiotemporal fluctuations in the suitability and/or connectivity of ephemeral wetlands, which are particularly sensitive to climate change and anthropogenic encroachment (Johnson et al., 2010). Understanding how wetlandscapes will evolve in response to these changes, and evaluating their ability to sustain the critical ecosystems that they contain, are vital for conservation and policy purposes.

Process-based hydrological models are an important set of approaches to support that effort. Recent work has advanced the ability of models to explicitly capture hydrological processes at the local scale, including cascading surface water fill-spill processes (Evenson et al., 2018; Shaw et al., 2013), wetland recharge and discharge in relation to downstream waters (Ameli & Creed, 2017; Evenson et al., 2018), and local surface water-groundwater exchanges between wetlands and their surrounding upland areas (Jones et al., 2018: McLaughlin et al., 2014; Shaw et al., 2013). These recent efforts led to enhanced simulation of wetland processes, and therefore improved potential to quantify aggregate impacts of wetlands at the catchment or landscape scales (Cohen et al., 2016; Evenson et al., 2016; Liu & Schwartz, 2011). Process-based models are promising in their ability to distinguish the effects of climate change and anthropogenic alterations (e.g., urbanization, intensive agriculture, landscape drainage, and groundwater pumping) on the spatio-temporal dynamics of changing wetlandscapes. A proper representation these dynamics, which determine habitat suitability (e.g., through metapopulation capacity), is critical for conservation and management of aquatic and semiaguatic species (Semlitsch & Bodie, 1998; Werner et al., 2007). However, this requires that (i) the most salient hydrological processes that govern wetlandscape dynamics at the landscape scale are adequately identified, and (ii) the model parameters corresponding to these processes are estimated. In practical applications, the cost and logistical efforts involved in monitoring single wetlands (let alone complete wetlandscapes) are substantial (Maleki et al., 2018), and in situ data are generally missing for these two conditions to be rigorously verified. Instead, model development and calibration is often based on monitoring data from a small subset of wetlands (Bertassello et al., 2022), or hermeneutic relationships to ancillary data (Brice et al., 2022). This practice raises the need to determine whether (and

under what conditions) the arbitrary and sparse sample of instrumented wetlands is representative of the full population of wetlands in the considered wetlandscape. It also raises the need for a direct approach to develop and calibrate hydrological models of wetlandscapes using observation data at the commensurate (i.e., landscape) scale.

By providing a consistent space-time representation of the earth system, images from spaceborne and airborne sensors are uniquely able to monitor water variables at the scale of the landscape to attribute hydrological change (Levy et al., 2018; Müller et al., 2016; Penny et al., 2022). Yet they entail fundamental tradeoffs between spatial resolution, temporal frequency, spatio-temporal coverage and detection ability. These tradeoffs are particularly relevant for wetlandscapes because the smallest wetlands are often the most frequent, the most hydrologically variable, and the hardest to detect using remote sensing imagery (Hondula et al., 2021). For example, Wu et al. (2019) combines high resolution aerial images from the National Agriculture Imagery Program (NAIP) of the United States Department of Agriculture with high accuracy LiDAR-based digital elevation models. The resulting maps of wetland inundation are highly accurate with a spatial resolution of 1 m, but the annual frequency of acquisition is too coarse to capture hydrological dynamics at (sub-annual) ecologically relevant time scales. In contrast, the Moderate resolution imaging spectro-radiometer (MODIS) missions offer daily global imagery that can capture these dynamics, but at a spatial resolution (200 m) that is too coarse to capture small but eco-hydrologically significant wetlands. To address this tradeoff, optical and Synthetic Aperture Radar (SAR) imagery from the Sentinel program (Sentinel 2 and Sentinel 1, respectively) have been used to map open water at both high resolution (10-60 m) and temporal frequency (10-12 days) (Kaplan & Avdan, 2017; Muro et al., 2016; Pérez Valentín & Müller, 2020). However, with launch dates between 2014 and 2016, the coverage period of Sentinel imagery is limited, whereas a sufficiently large sample of high-quality observations is necessary to ascertain and attribute change with adequate statistical power (Müller & Levy, 2019).

By providing 30-m resolution, weekly to bi-weekly, global multispectral scenes dating back to the early 1980s the various Landsat missions are a promising source of data to address these various tradeoffs. Landsat imagery has been widely used to monitor wetland dynamics (Frohn et al., 2009; Han et al., 2015; Huang et al., 2014; Kayastha et al., 2012; Mao et al., 2020; Sader et al., 1995) and to calibrate process-based models of catchments that contain a dense population of wetlands (Evenson et al., 2018; Lee et al., 2018). Yet cloud cover and image quality issues have limited their use for the short spatial and temporal scales that are ecologically relevant for wetlandscapes with ephemeral wetlands. More recently, new gap-filling algorithms have been proposed with promising ability to detect open water on Landsat images in cloudy weather (Mullen et al., 2021; Schwatke et al., 2019; Zhao & Gao, 2018), but their potential to improve the monitoring of wetlandscape dynamics at the relevant spatial and temporal scales remains to be evaluated. This paper fills this gap by comparing gap-filled water cover estimates from Landsat to two alternative data sources-namely in situ observations and

metric-resolution imagery—each time focusing on a key application and the most relevant tradeoff.

First, we focus on the tradeoff between spatial coverage and detection accuracy as it pertains to calibration data for hydrological models of wetlandscapes. On the one hand, gap-filled water cover estimates derived from gap-filled Landsat imagery offer a landscapescale perspective but are potentially impeded by water detection errors that might undermine a proper calibration of the hydrological model. On the other hand, in situ-observations of water stage provide (relatively more) accurate measurements of water extents, but only for a limited sample of instrumented wetlands. The hydrological dynamics of these instrumented wetlands may or may not be representative of that of the wetlandscape that the model is intended to capture. The extent to which the sampling error of in-situ observations compares with the measurement error of remote sensing observations determines the preferable data source for model calibration. We investigate this matter over various spatial scales by comparing the performance of a hydrological model calibrated using remote sensing wetlandscape observations with that of the same model calibrated using in-situ observations of a sparse sample of wetlands.

Second, we evaluate the tradeoff between spatial resolution and temporal frequency as it pertains to the ability to characterize the metapopulation carrying capacity of wetlandscapes. On the one hand, the spatial resolution of Landsat imagery (30 m) restricts its ability to monitor small (<1 ha or 10 Landsat pixels) but potentially ecologically significant wetlands. On the other hand, these features are captured by higher ( $\sim$ 1 m for NAIP; Wu et al., 2019) resolution imagery whose limited temporal coverage and low frequency (due to high acquisition costs) might fail to capture important temporal dynamics that occur over shorter (sub-annual) time scales. We compared the two data sources (Landsat and NAIP) based on their ability to evaluate the metapopulation capacity of a subset of the Prairie Pothole Region. The metapopulation capacity is an important ecological indicator that describes the habitat suitability of wetlandscapes (Bertuzzo et al., 2015). It is temporally variable and determined by the distribution of both the sizes individual wetland habitats and the distances separating them (Bertassello et al., 2021), two characteristics whose estimation is strongly affected by pixel resolution.

The manuscript is organized as follows. Section 2 describes the study regions. Section 3 describes the remote sensing procedure to monitor wetlandscape inundation (Section 3.1), the hydrological model and its calibration (Section 3.2) and the metapopulation capacity and its relation to wetlandscape dynamics (Section 3.3). Results are discussed in Section 4. The remote sensing calibration of the hydrological model is described and interpreted in Section 4.1. The relative salience of sampling and detection errors are discussed in Section 4.2, where the hydrological model is calibrated using different subsamples of the wetlandscape. Considerations regarding the spatial resolution and temporal coverage of remote sensing data sources are discussed in Section 4.3 by comparing metapopulation capacities predicted using alternative imagery sources with high (low) spatial resolution and low (high) temporal coverage.

# 2 | SITE DESCRIPTIONS

# 2.1 | Prairie Pothole Region

We focus on a 20 × 20 km domain within the Prairie Pothole Region in the Northern Great Plains of the United States (Figure 1) as a highly studied (Bertassello et al., 2021; Euliss et al., 2004; Wu et al., 2019) and ecologically significant wetlandscape with a (comparatively) high volume of available in-situ observations. The Prairie Pothole Region, PPR, is a spatially heterogeneous region with thousands of shallow wetlands known as potholes. These wetlands are important breeding areas for migratory waterfowls and other wetlanddependent wildlife, such as amphibians (Bertassello et al., 2021). In-situ monitoring data was obtained for 16 wetlands in the Cottonwood Lake Study Area (CLSA) which is located in south-central North Dakota. The CLSA has been the focus of biological, hydrological, and geochemical research and is an important U.S. Fish and Wildlife Service Waterfowl Production Area (Winter & LaBaugh, 2003). We used monitoring data for water level (staff gauges) located in each wetland at weekly intervals from April to October of each year from 2000 to 2015, when the wetland was ice-free (Mushet et al., 2016; Mushet & Solensky, 2018).

#### 2.2 | Texas Plava Lakes

The second considered wetlandscape is a  $20 \times 20$  km domain within the Texas Playa Lakes (TPL) region in the Southern High Plains of Texas (Figure 1). Playa Lakes are circular intermittent wetlands, which shape and size are comparable across the landscape. This configuration contrasts with the highly spatially heterogeneous nature of the PPR. Wetlands in the TPL provide important ecological services (e.g., flood control) and serve as key recharge zones for the underlying High Plains Aquifer system (Reeves & Reeves, 1996). We were not able to obtain any situ observations of stage or water extent for individual wetlands in the TPL (see Ganesan et al., 2016). This situation of low data availability is typical of most global wetlandscapes.

#### 3 | METHODS

# 3.1 | Remote sensing

Landsat 7 top-of-atmosphere (TOA) reflectance images (Collection 1 Tier 1) were acquired using Google Earth Engine (GEE) (Gorelick et al., 2017). To discriminate clouds from clear-sky pixels, we used a cloud score algorithm readily available in GEE that computes a simple cloud-likelihood score ranging from 0 to 100 using a combination of brightness, temperature and the Normalized Difference Snow Index (NDSI) (see <a href="https://developers.google.com/earth-engine/Landsat">https://developers.google.com/earth-engine/Landsat</a>). Following Huang et al. (2017), we identified as cloudy (or 'masked') pixels which score was greater than 10.

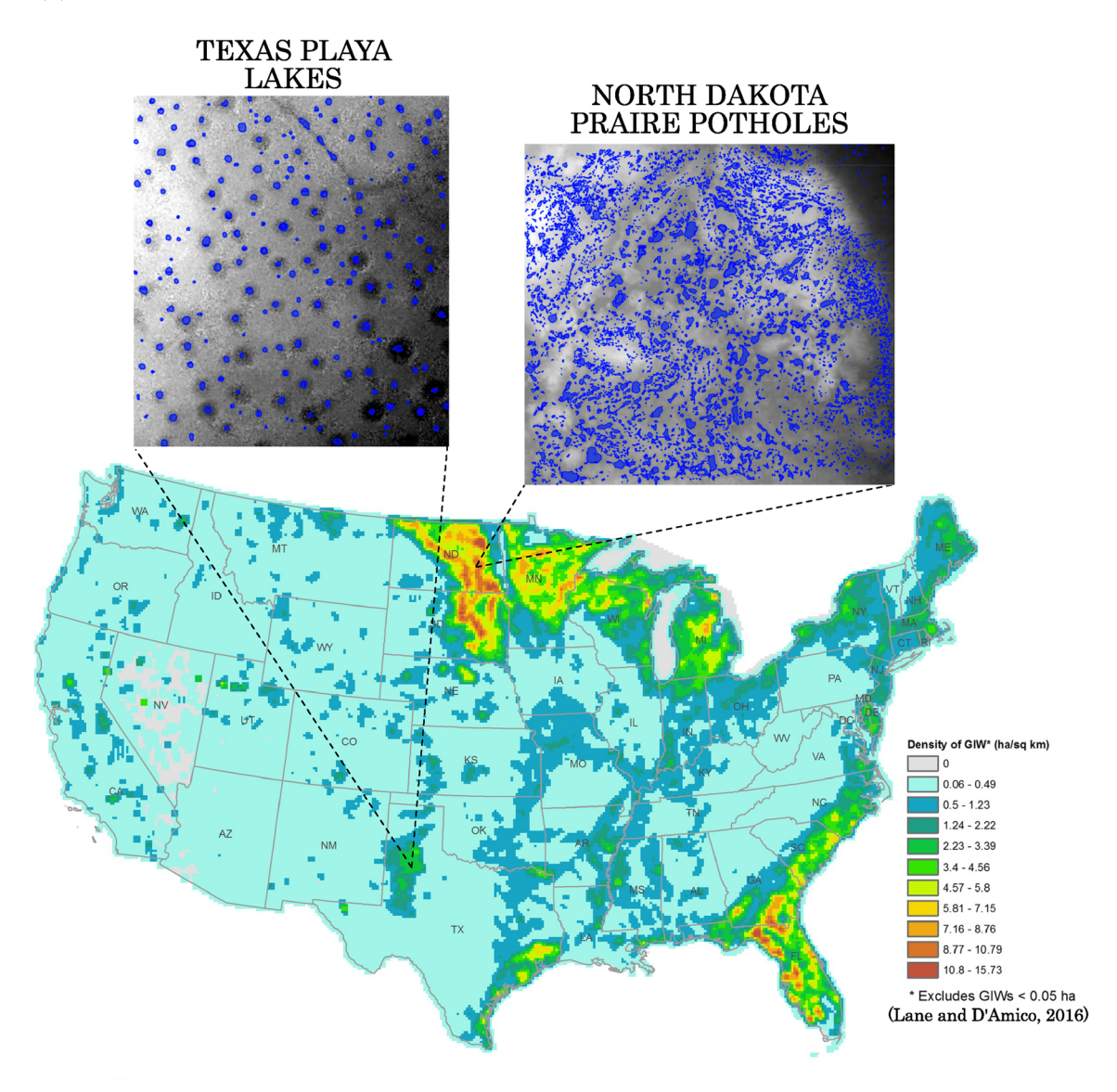


**FIGURE 1** Location of the studied wetlandscapes. The base map displays the estimated density of geographically isolated wetlands in the United States, adapted from Lane and D'Amico (2016)

Once the clouds masked out, we proceeded to classify the remaining pixels into land or open water based on their Modified Normalized Difference Index (MNDWI) (Han-Qiu, 2005):

MNDWI = 
$$\frac{B2 - B5}{B2 + B5}$$
,

where, *B*2 and *B*5 represent the green and Short-wave infrared bands of the Landsat 7 Enhanced Thematic Mapper sensor (ETM+). The MNDWI leverages the proclivity of water to preferentially reflect and absorb the green and short wave infrared frequencies of the electromagnetic spectrum, respectively. We segmented the MNDWI images into 'dry' and 'wet' pixels by using a k-means clustering algorithm (Arthur & Vassilvitskii, 2006). The accuracy of unsupervised classification is sensitive to the relative number of pixels assigned to each of the two clusters, so the automatic identification of a segmentation

threshold can be problematic for images dominated by either land or open water. Following Mullen et al. (2021), we addressed this issue by (i) automatically classifying each image using k-means, (ii) recording the segmentation threshold (i.e., the MNDWI level above which a pixel is classified as water) for each image and (iii) using the median value of the obtained segmentation thresholds to segment *all* the images.

We then used the approach described in Mullen et al. (2021) to transform the three-class images ('masked', 'dry' and 'wet') into binary water extent images ('dry' and 'wet'). Note that the 'masked' pixel class includes both the pixels masked by clouds and the pixels with no data due to the scanline corrector failure on Landsat 7 images taken after September 2003. The algorithm infers the inundation status of cloudy pixels using a supervised classification to relate the inundation status of unmasked pixels to their inundation frequency, that is, the fraction of time each pixel is inundated in the set of images where it is unmasked.

over the (constant) catchment area  $A_{c,i}$ . The second term accounts for the volumetric water loss from the wetland at a time-averaged potential evapotranspiration rate ET over a contributing water surface area  $A_i$  that changes over time. The third term quantifies the volumetric water loss from the wetland to the connected aquifer. This process occurs throughout the (time-varying) wetted area of the pool  $S_i$  and is modulated by the recession constant  $K_{s,i}$ . Although expressed in Equation (1) as a function of wetland volume V, the wetlandscape dynamics captured in the water balance could equivalently be expressed as a function of water extent surface area A or wetland stage h if the relationship between these three variables is known. This relationship is determined by wetland bathymetry and is approximated as described in Supporting Information S1.

The model was implemented using the National Wetland Inventory map (Cowardin & Golet, 1995) as representative of the maximum spatial extent of the wetlands. We modelled the daily hydrological dynamics in each wetland (given as either V, h, or A) by integrating

Time series of binary inundation images were finally analysed using dedicated GEE functions to obtain both the size distribution of continuous inundation patches in a given images, and the time series of total inundated area for a given (e.g.,  $20 \times 20$  km) footprint. The full procedure used to obtain water extent time series of a given domain is available as a self-contained GEE script at https://code.earthengine.google.com/0578e09e7fecab4ca3171da29158cd1c.

We obtained annual 1 m resolution (compared to 30 m for Landsat) classified binary inundation images of the PPR for the 2009-2017 period from Wu et al. (2019) for an approximately  $10 \times 20$  km subset of the considered domain. We used this dataset both to evaluate our classification output and to investigate the spatial versus temporal resolution tradeoff discussed in Section 4.3. The validation dataset combines aerial images from NAIP with high accuracy LiDAR-based digital elevation models. These annual images represent wetland water extents in the PPR when the NAIP image is captured, which is typically sometime between May and July, and is taken as representing growing season conditions. To evaluate the performance of our own classification outcomes, we selected the classified Landsat image with acquisition date closest to that of the NAIP image. We then generated a random set of 5000 control points and compared the classes ('dry' or 'wet') predicted by the two images at that location. Classifications from the two data sources (Landsat 7 or NAIP) matched with an accuracy ranging between 89% and 97% for the 6 years when the two data sources overlapped.

3.2 | Hydrological model

Water extent estimates (obtained from remote sensing or in situ observations) were used to calibrate the process-based model of wetlandscape hydrological dynamics developed in Bertassello et al. (2019). Therein, the landscape is considered as populated by distributions of independent wetlands, all sharing identical stochastic precipitation inputs (P) and evapotranspiration losses (PET), and all exchanging water with shallow groundwater. The model neglects the spatial variability of hydro-climatic forcing, which at the considered spatial scales ( $\simeq 400 \text{ km}^2$ ) are likely to have much smaller impact on hydrological dynamics than temporal hydroclimate fluctuations. All wetlands are assumed connected to a shallow groundwater for which they act as a recharge sources, thus water tends to move from the wetland into the shallow aguifer. Note that wetlands in the considered regions do not significantly contribute to regional subsurface groundwater flow paths (Brooks et al., 2018; Winter & Rosenberry, 1995). Given these assumptions, each wetland i of the wetlandscape satisfies the water-balance equation:

$$\frac{dV_i}{dt} = (P+N)A_{c,i} - ETA_i(V_i) - K_{s,i}S_i(V_i), \tag{1} \label{eq:decomposition}$$

where,  $\frac{dV_i}{dt}$  represent the change in water volume stored by wetland *i*. The first term on the right-hand side of Equation (1) represents water inputs due to a sequence of precipitation *P* and snowfall *N* events

The model was implemented using the National Wetland Inventory map (Cowardin & Golet, 1995) as representative of the maximum spatial extent of the wetlands. We modelled the daily hydrological dynamics in each wetland (given as either V, h, or A) by integrating Equation (1) and forcing it with daily precipitation and evapotranspiration (ET) data. We used daily precipitation data from the National Oceanic and Atmospheric Administration, NOAA, from the stations of Jamestown Municipal Airport, ND (USW00014919) and Abernathy, TX (USC00410012), respectively for the PPR and the TPL wetlandscapes. Following Huang et al. (2013) we modelled the form of precipitation as rainfall or snowfall based on the daily mean temperature obtained from the same station. When the average daily temperature is below 0°C, the falling precipitation is assumed to be snowfall (Carroll et al., 2005). Snowfall accumulates on the ground as snowpack, modelled in terms of snow water equivalent (SWE) using a snow-to-liquid ratio of 10:1 (Mekis & Brown, 2010). Following Carroll et al. (2005) and Huang et al. (2013), snowpack melting was modelled with the degree-day method as  $N_t = 0.274 T_t$ , where  $N_t$  is the snowmelt depth (m) on day t that runs off into the pond,  $T_t$  is the mean daily temperature (°C) and 0.274 is the approximate degree-day ratio  $(cm \circ C^{-1} d^{-1})$ . When  $T_t < 0 \circ C$ ,  $N_t = 0$  (i.e., no snowmelt). Air temperature was also used estimate potential evapotranspiration, PET, using the Thornthwaite method. We modelled the temporal hydrologic dynamics for each of the wetlands identified by the NWI map within the considered  $20 \times 20 \, \text{km}$  domain. We then used the daily time series of stored water volumes to estimate wetland areas using the relationships described in SI, which we aggregated to obtain daily time series of total inundated area in the wetlandscape,  $A_T$ . We calibration the recession constant, K<sub>s,i</sub>, manually by comparing the modelled and observed time series of  $A_T$ .

# 3.3 | Metapopulation capacity

In classical metapopulation theory (Hanski & Ovaskainen, 2000), the metapopulation capacity,  $\lambda_{max}$ , captures the impact of landscape complexity, that is the amount of patch habitat and its spatial configuration, on metapopulation persistence. This key index can be evaluated as the leading eigenvalue of the patch-landscape matrix M, derived from the Jacobian of the system J=cM-el (Bertuzzo et al., 2015;

10991085, 2022, 11, Downloaded from https://onlinelibrary.wiley.com/doi/10.1002/hyp.14739 by University Of Notre Dame, Wiley Online Library on [17/04/2023]. See the Terms

and Conditions (https://onlinelibrary.wiley

and-conditions) on Wiley Online Library for rules of use; OA articles are governed by the applicable Creative Commons

Hanski & Ovaskainen, 2000), where c and e are respectively the colonization and extinction rate of a given species. The matrix M contains information about the landscape and the quality of the patches and its elements,  $m_{ii}$ , are defined as:

$$m_{ij} = exp\left(-d_{ij}(t)/D\right)A_i(t)A_j(t) \tag{2}$$

For wetlandscapes, where wetlands play the role of habitat patches,  $A_i$  ( $L^2$ ) is the surface area of wetland i,  $d_{ij}$  (L) is the shortest distance between wetlands i and j and D (L) is the dispersal ability of the considered species. Thus, combined with the hydrological model that explicitly predicts connectivity (represented by inter-wetland distance  $d_{ij}$ ) and habitat suitability (represented by wetland area  $A_i$ ) as functions of time and hydroclimatic inputs, this approach can be used to model the effect of the spatiotemporal dynamics of wetlandscapes on habitat availability and accessibility for any considered focal species (Bertassello et al., 2021). It is worth noting that here wetland area is used as a surrogate metric for wetland habitat carrying capacity. However, several factors other than water area, such as water depth, water temperature, salinity, and aquatic plant types and coverage, might drive habitat suitability as well and can potentially be integrated into our approach.

### 4 | RESULTS AND DISCUSSION

# 4.1 | Calibration results

Figure 2 shows model calibration results using remotely sensed water cover as calibration data for the considered  $20 \times 20$  km domains in the PPR (left) and TPL (right). Figure 2b shows water cover time series estimated from Landsat 7 (red) and predicted by the model (blue) using precipitation inputs displayed in Figure 2a. Figure 2c which displays the histogram and empirical complementary cumulative density functions of total water cover across observation dates. Out-of-sample validation results against 5 additional years of data in the PPR and 3 additional years of data in the TPL are presented in SI (Figure S5).

Calibration results in the two wetlandscapes show distinct hydrological behaviours. In the PPR, the hydrological regime is persistent (Botter et al., 2013) with water present in the wetlandscape for nearly all predictions and observations. This is especially true during the *wet* period ranging from April to October where the comparison between the output of the model and the remote sensing data is possible. During the remaining part of the year, the wetlandsape is covered by snow, which both prevents an accurate detection of open water surfaces using remote sensing (Acharya et al., 2018) and limits suitability as an aquatic habitat. Results suggests that model predictions (blue) overestimate the total water extent area in the wetlandscape between 2005 and 2010, when compared to the remote sensing estimates used to calibrate it (red). This period has also seen an overall reduction of the Palmer Hydrological Drought Index (see Figure S2). This decrease in PHDI arises in the precipitation and

evapotranspiration data forcing the hydrological model but was not visible in the observed water extents. This points to factors affecting the PHDI and wetland water extents that are not included in the model. In particular, the model does not incorporate anthropogenic alteration. A substantial amount of pumping was documented at Devil's Lake in the vicinity or our domain, starting mid-year 2005 and ending in 2010 (McKenna et al., 2017; Todhunter, 2016), which might have induced a temporary decrease in wetlandscape water levels. This decrease is reflected in persistent negative monthly gravitational anomalies starting in the summer of 2006 through 2009, from the GRACE Tellus Monthly Mass Grid in the PPR study area (see Figure S4). Thus, anthropogenic alterations are visible in the discrepancy between model predictions and observed water extents. Note that this insight is specifically enabled by the landscape scale of the calibration data obtained from satellite imagery. It illustrates the potential to identify landscape-scale hydrologic processes that might be omitted by the current model, which can be leveraged within an iterative model design process.

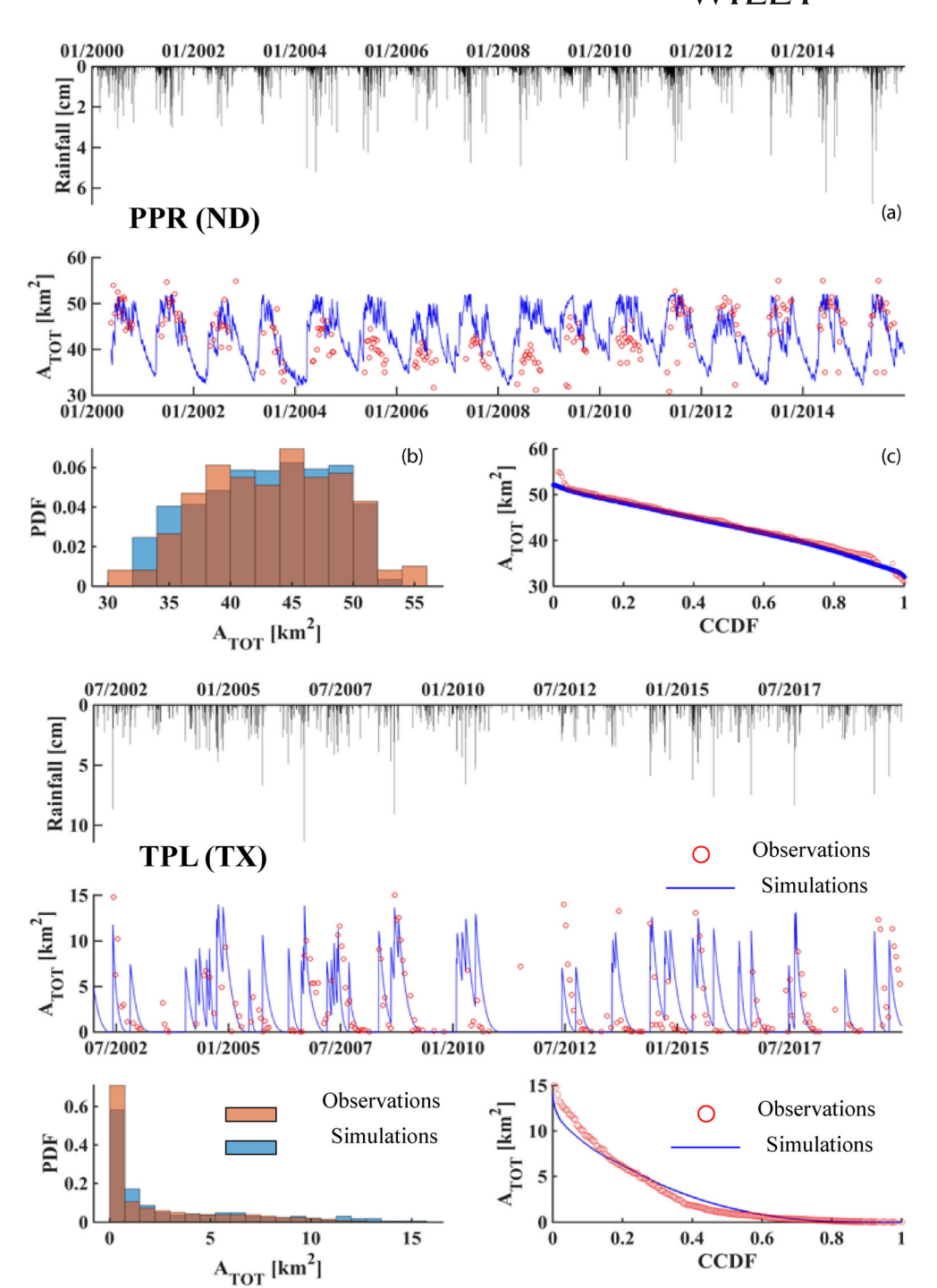
The wetlandsacpe hydrological regime is comparatively more erratic in the TPL, where the wetlandscape is completely dry for a substantial portion of the year. This erratic regime arises for two important reasons. First, evapotranspiration and infiltration processes play a significant role in the water balance dynamics of the wetlandscape. Rainfall intensity has to exceed comparatively larger thresholds than in the PPR to cause runoff events that inundate or flood the playa lakes (Thompson et al., 1994). Second, wetlands are located in a heavily cultivated region using groundwater as main irrigation source. Groundwater pumping contributes to draining the groundwaterconnected playa lakes between rainfall events. While the hydrological model results shows a good agreement with remote sensing calibration data during intense rainfall events (Figure 2), discrepancies are generally larger during smaller events where the model overestimates water cover. In addition to groundwater pumping, further analysis using 3-m resolution daily imagery from Planet Labs has shown that this discrepancy could also be caused by challenges in detecting small and shallow bodies of water formed by turbid agricultural runoff on Landsat 7 satellite imagery (see Figure S3).

#### 4.2 | Sampling versus detection error

Monitored wetlands are equipped with water stage measuring gauges and (assuming their bathymetry is well characterized) are not subject to the type of measurement errors obtained for remotely sensed water cover estimates. However, using in-situ observations from individual wetlands to calibrate landscape-scale models requires that the water extent fluctuations observed for the sampled wetlands are representative of the wetlandscape dynamics captured by the model. The extent to which the sampling error of in situ observations compares to the measurement error of remote sensing observations determines which data source is preferable to calibrate hydrological models.

We investigated this question in the PPR wetlandscape, where stage observations were available for a sample of 16 instrumented

FIGURE 2 Calibration results for hydrological model of the wetlandscape in the Prairie Pothole Region (PPR, top) and the Texas Plava Lakes (TPL. bottom). (a) Daily precipitation time series used as modelling input. (b) Time series of daily water extents within the considered 20 × 20 km domains. Predictions from the calibrated model are represented in blue and calibration data obtained from Landsat 7 are represented in red. (c) Histogram and empirical complementary **Cumulative Distribution Function** of predicted (blue) and observed (red) daily domain-wide water extents



wetlands (orange in Figure 3). We used these in-situ data to calibrate the model and the resulting predicted time distribution of daily water extent within the  $20 \times 20$  km domain are displayed in dashed orange in Figure 3, where the corresponding *observed* distribution obtained from remote sensing is displayed as a pink histogram. We replicated the exercise this time using water extent estimates of the 16 wetlands observed from remote sensing to calibrate the model, with predicted distribution displayed in solid orange on Figure 3.

Comparing the two modelled distributions to each other informs on the effect of detection errors on the calibrated model output: discrepancies between the water extent of the 16 calibration wetlands obtained using stage measurement and remote sensing observations have a visible effect on model prediction. However, this effect is dwarfed by the effect of sampling errors. The model calibrated with observations (whether remotely sensed or in situ) from the arbitrary wetlands underestimate both the variance and the average water cover of the wetlandscape. To determine the extent to which this discrepancy is associated with this specific sample of instrumented wetland, we replicated the analysis using remote sensing water cover estimates from three randomly located  $5\times 5$  km subdomains (black on Figure 3). Using these datasets to calibrate the model introduced much larger negative biases in the predicted distributions of daily

**FIGURE 3** (a) Representative water extent obtained from the National Wetland Inventory for the considered  $20 \times 20$  km domain in the Prairie Pothole Region. The three considered  $5 \times 5$  km subdomains are outlined in black (solid, dashed, and dotted). The 16 instrumented wetlands located in the Cottonwood Lake Study Area, CLSA, are represented in orange in the detail. (b) Histograms and kernel density estimates (KDE, bandwidth =  $2 \text{ km}^2$ ) of the distribution of daily total water cover in the  $20 \times 20$  km domain. The pink histogram is constructed using remote sensing observations and the different KDE curves are constructed using water extent predictions from models calibrated using (i) in-situ observations from the 16 wetlands (dashed orange), (ii) remote sensing observations from the 16 wetlands (plain orange), (iii) remote sensing observations from different  $5 \times 5$  km subdomains (black) and remote sensing observations from the full  $20 \times 20$  km domain (blue). Blue kernel density estimate was constructed using model predictions. (c and d) Equivalent results for the Texas playa Lake wetlandscape (KDE, bandwidth =  $1 \text{ km}^2$ )

water extents in the  $20 \times 20 \text{ km}$  domain (dotted, dashed and solid black lines on Figure 3).

In contrast to PPR, the TPL wetlandscape is characterized by lower spatial heterogeneity, with all the playa lakes having comparable shapes and sizes. Under these conditions a model calibrated using remotely sensed water extents from a  $5\times 5$  km subdomain (black) performs similarly to a model calibrated using the remotely sensed data from the full  $20\times 20$  km domain (blue). Given the detection challenges discussed in the previous section, this suggests that a model calibrated using a sample of approximately 20 instrumented playa lakes (the approximate number of wetland in a  $5\times 5$  km subdomain) might perform equivalently—or even outperform—a model calibrated using landscape-scale remote sensing data. Unfortunately, in situ data are not available in the region to rigorously test this hypothesis.

# 4.3 | Spatial resolution versus temporal coverage

Remote sensing data implies an inherent tradeoff between the spatial resolution and spatial coverage. Satellites providing very high

(~meter) resolution images were, for the most part, launched within the last decade, which limits the temporal coverage of the obtained water cover estimates. Very high resolution imagery is also typically costly to acquire, which limits the frequency of water cover information that can be obtained. For example, the NAIP imagery used in Wu et al. (2019) to create 1-m resolution water cover for the PPR is only acquired once per year. In contrast, publicly available satellite imagery from the Landsat 7 mission provides bi-weekly global images of the earth surface since 1998 at no cost to the user. However, their spatial resolution of 30 m is much coarser. Navigating this tradeoff is particularly important for ecological processes in wetlandscapes, where both the spatial and the temporal dynamics of water cover play a critical role.

In a spatially heterogeneous landscape like the PPR, 30-m resolution imagery might miss specific features of the landscape with disproportionate ecological importance. In Figure 4, we compare a water cover mask obtained from 30-m resolution Landsat imagery (red) to a 1-m resolution water cover mask estimated by Wu et al. (2019) for the same month (August 2017) using very high resolution NAIP imagery. The two water cover masks are compared based on the size distribution of contiguous water patches (Figure 4b) and the distribution

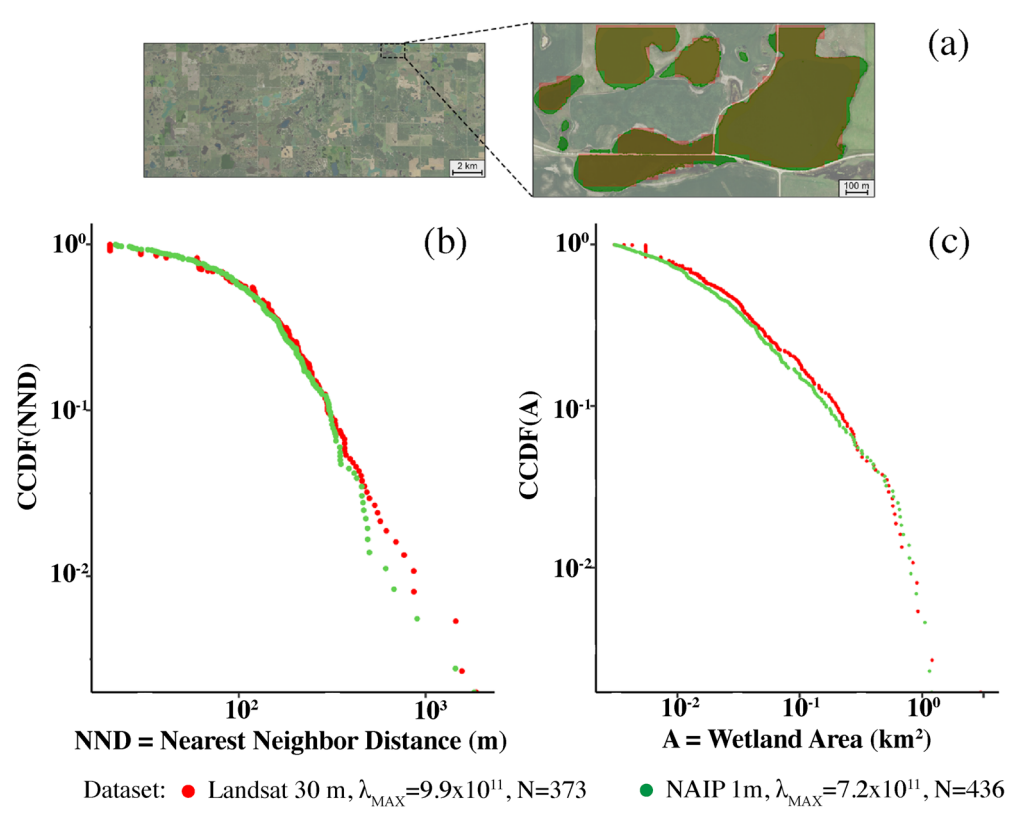


**FIGURE 4** (a) Detail of the Prairie Pothole Region wetlandscape in August 2017 showing the water cover estimated from 30-m resolution Landsat 7 imagery (red) and the 1-m resolution water cover obtained from Wu et al. (2019). The 30-m resolution mask misses several small wetlands and fails to fragment the large wetland along the E-W road on the bottom left corner of the detail. (b) Empirical Complementary Cumulative Distribution Function of wetland size distribution in August 2017 for the approximately  $20 \times 10$  km footprint of the Pairie Pothole Region analysed in Wu et al. (2019). Results obtained from the 30-m resolution water mask created from Landsat 7 and the 1-m resolution water mask obtained from Wu et al. (2019) are given in red and green, respectively. (c) Empirical Complementary Cumulative Distribution Function equivalent to panel (b), but representing the nearest distance between neighbouring wetlands, rather than wetland sizes

of the distances between the nearest patches (Figure 4c). These two distributions respectively represent the suitability and connectivity of the habitat for aquatic species and drive the metapopulation capacity of the wetlandscape, as described in Equation (2). As seen in the details displayed on Figure 4b, the 30-m resolution mask underestimates the fragmentation of the wetlandscape by missing small obstacles like dikes and causeways. It also misses small wetlands that might serve as stepping stones for migrating species and increase habitat connectivity. These misclassifications are small in terms relative area error, but they have a strong impact on the distributions of water patch areas, (most visibly) inter-patch distances and habitat patch occupancy. Overall, classification errors associated with a 30-m resolution water mask cause the metapopulation capacity to be overestimated by approximately 135% for that particular image (August 2017), compared to the corresponding 1-m resolution water mask.

On the other hand, temporal dynamics in the PPR are substantial with seasonal variations of total water cover of about 30% of their long term average (Figure 2b). These fluctuation also affect the distribution of water patches within the landscape, as large wetlands fragment into multiple components when draining (Figure S3) (Bertassello et al., 2020). This causes variations in habitat suitability and

connectivity that are reflected in substantial fluctuations of metapopulation capacity (see Equation (2)). Figure 5 displays metapopulation capacity values computed for water extent estimates obtained from all cloud-free Landsat 7 images obtained for the PPR wetlandscape between 2000 and 2021. Metapopulation capacities were computed for species with dispersal distanced *D* of 200 m (green) and 1000 m (red), respectively. Equivalent metapopulation capacities computed using the 1-m resolution water masks from Wu et al. (2019) are displayed based on the acquisition date of the NAIP imagery.

Depending on the year and species dispersal distance, we found that the error on the metapopulation capacity obtained from Landsat images ranges from 15% to 22%, compared to the 'true' metapopulation value obtained from the 1-m resolution water mask obtained for the same date. However, this spatial resolution error is dwarfed by the annual (Figure 5a) and seasonal (Figure 5b) variability of metapopulation capacities that arises from strong temporal variations in wetlandscape water cover. Extreme water cover conditions (dashed black line on Figure 5a) can cause the metapopulation capacity to nearly double, compared to a rolling central tendency obtained from non-parametric LOESS regression (solid coloured lines on Figure 5a). In fact, most metapopulation capacity values obtained from 1-m

1099/1085, 2022, 11, Downloaded from https://onlinelibarry.wiley.com/doi/10.1002/hyp.14739 by University Of Notre Dame, Wiley Online Library on [17/04/2023]. See the Terms and Conditions (https://onlinelibrary.wiley.com/terms-and-conditions) on Wiley Online Library for rules of use; OA articles are governed by the applicable Creative Commons

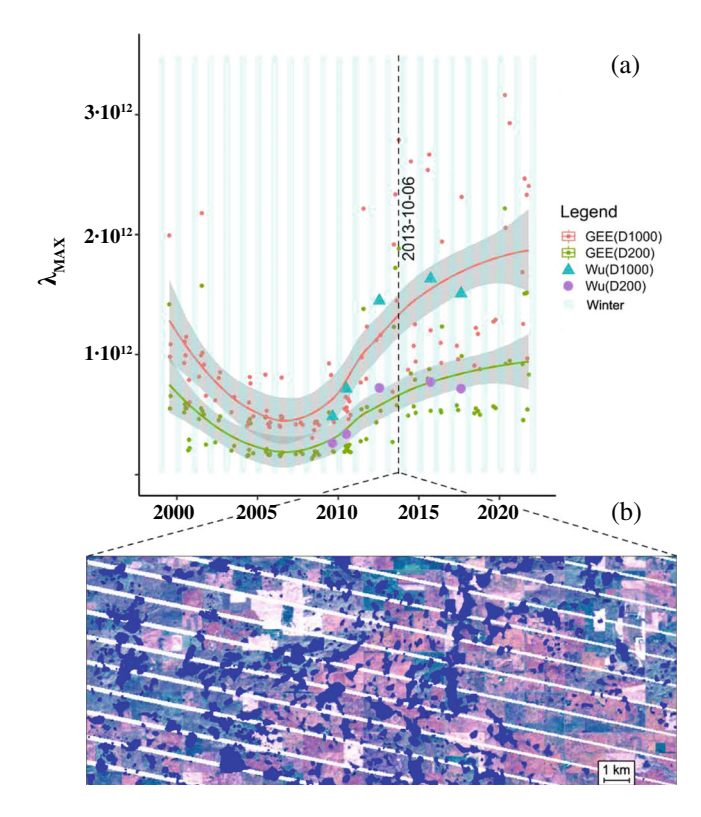


FIGURE 5 (a) Time series of metapopulation capacity  $\lambda_{max}$ obtained from 30-m resolution Landsat-based water extent estimates (red and green) and from the 1-m resolution water masks derived in Wu et al. (2019) (blue and purple). Metapopulation capacities were estimated using dispersal distances of  $D = 200 \,\mathrm{m}$  and  $D = 1000 \,\mathrm{m}$  for purple and green symbols and for red and blue symbols, respectively. Solid lines represent non-parametric (LOESS) regression estimate with a bandwidth of 30 days, with grey-shaded areas representing the corresponding 95% confidence intervals. Blue vertical columns represent winter months (November-April), where no usable remote sensing observation were available. (b) Landsat 7 real colour background with gap-filled water classification (blue) for October 6, 2013, when  $\lambda_{max}$  is approximately double its LOESS regression estimate. No clouds can be seen on the image

resolution water masks are within the 95% confidence interval of LOESS-regressed results obtained from the 30-m resolution data.

Overall this suggests that, for the PPR wetlandscape, the benefits arising from Landsat 7's ability to capture temporal variations of metapopulation capacity might exceed the errors arising from its inability to capture spatial details of the landscape. Changes in size, shape and connection of habitat patches induced by changes in water level may generate ecological opportunities due to transient windows for connectivity (Bertassello et al., 2021; Rinaldo & Rodriguez-Iturbe, 2022). Therefore, being able to characterize these transient wetlandscape conditions is of key importance for many ecological investigations.

#### 5 **CONCLUSIONS**

This paper evaluates the potential for using landscape-scale remote sensing water cover estimates to calibrate hydrological models of

wetlandscapes. We showed that the current prevailing procedure of using in-situ data from a small and arbitrary subset of instrumented wetlands for calibration introduces a substantial error in model predictions of water extents. In the Pairie Pothole Region, this sampling error substantially exceeds the error associated with detecting water on remote sensing imagery. This suggests that remote sensing stands out as a promising calibration data source for landscape-scale models in spatially heterogeneous wetlandscapes. Our results also suggests that wetlanscape-scale dynamics can be adequately captured by a small number of monitored wetlands in homogeneous landscapes like the Texas Playa Lakes, where water was also incidentally more challenging to detect on remote sensing imagery.

The large variability in wetland areas across the PPR makes it more challenging to fully capture the inundation dynamics from smaller domain sizes. This is particularly true when the domain is characterized by an abundant fraction of small wetlands that might be not detected because they are often optically complex, obscured by vegetation, or below the resolvable size of satellite sensors (DeVries et al., 2017). These small water bodies are also of key importance for several landscape functions since they can facilitate the dispersal among suitable habitat (Semlitsch & Bodie, 1998) or they should not be overlooked in estimation of greenhouse gas emissions (Hondula et al., 2021). This suggests that the spatial heterogeneity of the PPR wetlandscape is such that care is needed in drawing ecological and biogeochemical conclusions (e.g., species persistence or methane emission) from limited spatial domains in complex and dynamic habitats.

In situations where landscape-scale remote sensing observations are beneficial, we proceeded to evaluate the tradeoff between spatial resolution and temporal coverage that is inherent to satellite image products. We found that a long running publicly available dataset (Landsat 7) was able to capture important ecologically relevant temporal dynamics of the Prairie Pothole Region that were missed by recent higher resolution (but lower temporal coverage) products. Nonetheless, limitations associated with the spatial resolution of Landsat are important to keep in mind. This is particularly true in wetlandscape with an abundant fraction of small wetlands that might be partially obscured by vegetation, or below the resolvable size of satellite sensors (DeVries et al., 2017). These small waterbodies might play a disproportionate role in the landscape in terms, for example in terms of facilitating species dispersal (Semlitsch & Bodie, 1998) or as biogeochemical carbon sources (Hondula et al., 2021). In that regard, recent and forthcoming high-frequency and high-resolution products have a particularly important role to play for the characterization of changing wetlandscapes. For instance, data from the NASA-ISRO SAR mission will provide repeat long-wavelength SAR imagery and thus play an important role in improving estimates of surface water dynamics; Surface Water and Ocean Topography (SWOT) mission will provide global scale data on surface water storage change. However, limitations associated with the limited temporal coverage of these products persists and call for more research into combining them with longer running products like Landsat. In addition, the ease of use is also a consideration when selecting remote sensing versus in-situ observations for model calibrations. While the former's availability is

MULLEN ET AL. WILEY 11 of 13

increasing, sometimes it is not readily used because (1) it is challenging to process for model use and (2) measurements taken by the imagery do not directly link to parameterization needed for a model.

Overall, our findings suggest that in-situ and remote sensing observations (whether of high resolution or long time coverage) have an important role to play in improving our understanding of wetlandscape dynamics and that the spatial heterogeneity of the landscape, and the temporal variability of its climate drivers, might play an important role in determining which wetlandscape will most benefit from investments into each data source.

#### **ACKNOWLEDGEMENTS**

PSCR involvement in this collaboration was supported, in part, by the Lee A. Reith Endowment in the Lyles School of Civil Engineering at Purdue University. Leonardo E. Bertassello and Marc F. Müller gratefully acknowledge financial support from the US National Science Foundation (EAR 2142967).

#### **DATA AVAILABILITY STATEMENT**

The data that support the findings of this study are publicly available. Data for wetland extent are available at the National Wetland Inventory website, while the precipitation and temperature data were obtained from National Oceanic Atmospheric Administration website. Remote sensing product were obtained from the Landsat 7 mission, and they have been analysed using Google Earth Engine (https://developers.google.com/earth-engine/landsat). The full procedure used to obtain water extent time series of a given domain is available as a self-contained GEE script at https://code.earthengine.google.com/0578e09e7fecab4ca3171da29158cd1c.

# ORCID

P. Suresh C. Rao (1) https://orcid.org/0000-0002-5982-3736

# **REFERENCES**

- Acharya, T. D., Subedi, A., & Lee, D. H. (2018). Evaluation of water indices for surface water extraction in a landsat 8 scene of Nepal. *Sensors*, 18(8), 2580.
- Acreman, M., & Holden, J. (2013). How wetlands affect floods. *Wetlands*, 33(5), 773–786.
- Ameli, A. A., & Creed, I. F. (2017). Quantifying hydrologic connectivity of wetlands to surface water systems. Hydrology and Earth System Sciences, 21(3), 1791–1808.
- Arthur, D., & Vassilvitskii, S. (2006). k-means++: The advantages of careful seeding (Tech. Rep.). Stanford.
- Bertassello, L. E., Bertuzzo, E., Botter, G., Jawitz, J. W., Aubeneau, A. F., Hoverman, J. T., Rinaldo, A., & Rao, P. S. C. (2021). Dynamic spatiotemporal patterns of metapopulation occupancy in patchy habitats. *Royal Society Open Science*, 8(1), 201309.
- Bertassello, L. E., Jawitz, J. W., Aubeneau, A. F., Botter, G., & Rao, P. S. C. (2019). Stochastic dynamics of wetlandscapes: Ecohydrological implications of shifts in hydro-climatic forcing and landscape configuration. *Science of the Total Environment*, 694, 133765.
- Bertassello, L. E., Jawitz, J. W., Bertuzzo, E., Botter, G., Rinaldo, A., Aubeneau, A., Hoverman, J. T., & Rao, P. S. C. (2022). Persistence of amphibian metapopulation occupancy in dynamic wetlandscapes. *Landscape Ecology*, 37(3), 695–711. https://doi.org/10.1007/s10980-022-01400-4

- Bertassello, L. E., Rao, P. S. C., Jawitz, J. W., Aubeneau, A. F., & Botter, G. (2020). Wetlandscape hydrologic dynamics driven by shallow ground-water and landscape topography. *Hydrological Processes*, 34(6), 1460–1474.
- Bertuzzo, E., Rodriguez-Iturbe, I., & Rinaldo, A. (2015). Metapopulation capacity of evolving fluvial landscapes. Water Resources Research, 51(4), 2696–2706.
- Botter, G., Basso, S., Rodriguez-Iturbe, I., & Rinaldo, A. (2013). Resilience of river flow regimes. *Proceedings of the National Academy of Sciences*, 110(32), 12925–12930.
- Brice, E. M., Halabisky, M., & Ray, A. M. (2022). Making the leap from ponds to landscapes: Integrating field-based monitoring of amphibians and wetlands with satellite observations. *Ecological Indicators*, 135, 108559.
- Brooks, J., Mushet, D., Vanderhoof, M., Leibowitz, S., Christensen, J., Neff, B., Rosenberry, D. O., Rugh, W. D., & Alexander, L. (2018). Estimating wetland connectivity to streams in the prairie pothole region: An isotopic and remote sensing approach. Water Resources Research, 54(2), 955–977.
- Carroll, R., Pohll, G., Tracy, J., Winter, T., & Smith, R. (2005). Simulation of a semipermanent wetland basin in the Cottonwood Lake area, East-Central North Dakota. *Journal of Hydrologic Engineering*, 10(1), 70–84.
- Cheng, F. Y., & Basu, N. B. (2017). Biogeochemical hotspots: Role of small water bodies in landscape nutrient processing. *Water Resources Research*, 53(6), 5038–5056.
- Cohen, M. J., Creed, I. F., Alexander, L., Basu, N. B., Calhoun, A. J., Craft, C., D'Amico, E., DeKeyser, E., Fowler, L., Golden, H. E., Jawitz, J. W., Kalla, P., Kirkman, L. K., Lane, C. R., Lang, M., Leibowitz, S. G., Lewis, D. B., Marton, J., McLaughlin, D. L., ... Walls, S. C. (2016). Do geographically isolated wetlands inuence land-scape functions? *Proceedings of the National Academy of Sciences*, 113(8), 1978–1986.
- Cowardin, L. M., & Golet, F. C. (1995). US fish and wildlife service 1979 wetland classification: A review. In *Classification and inventory of the world's wetlands* (pp. 139–152). Springer.
- Cronk, J. K., & Fennessy, M. S. (2016). Wetland plants: Biology and ecology. CRC Press.
- Dahl, T. E. (1990). Wetlands losses in the United States, 1780's to 1980's. US Department of the Interior, Fish and Wildlife Service.
- DeVries, B., Huang, C., Lang, M. W., Jones, J. W., Huang, W., Creed, I. F., & Carroll, M. L. (2017). Automated quantification of surface water inundation in wetlands using optical satellite imagery. *Remote Sensing*, *9*(8), 807.
- Dudgeon, D., Arthington, A. H., Gessner, M. O., Kawabata, Z.-I., Knowler, D. J., Lévêque, C., Naiman, R. J., Prieur-Richard, A. H., Soto, D., Stiassny, M. L., & Sullivan, C. A. (2006). Freshwater biodiversity: Importance, threats, status and conservation challenges. *Biological Reviews*, 81(2), 163–182.
- Erwin, K. L. (2009). Wetlands and global climate change: The role of wetland restoration in a changing world. Wetlands Ecology and Management, 17(1), 71–84.
- Euliss, N. H., LaBaugh, J. W., Fredrickson, L. H., Mushet, D. M., Laubhan, M. K., Swanson, G. A., Winter, T., Rosenberry, D., & Nelson, R. D. (2004). The wetland continuum: A conceptual framework for interpreting biological studies. Wetlands, 24(2), 448–458.
- Evenson, G. R., Golden, H. E., Lane, C. R., & D'Amico, E. (2016). An improved representation of geographically isolated wetlands in a watershed-scale hydro logic model. *Hydrological Processes*, 30(22), 4168–4184.
- Evenson, G. R., Jones, C. N., McLaughlin, D. L., Golden, H. E., Lane, C. R., De-Vries, B., Alexander, L., Lang, M., & Sharifi, A. (2018). A watershedscale model for depressional wetland-rich landscapes. *Journal of Hydrology X*, 1, 100002.
- Frohn, R. C., Reif, M., Lane, C., & Autrey, B. (2009). Satellite remote sensing of isolated wetlands using object-oriented classification of landsat-7 data. *Wetlands*, *29*(3), 931–941.

- Ganesan, G., Rainwater, K., Gitz, D., Hall, N., Zartman, R., Hudnall, W., & Smith, L. (2016). Comparison of infiltration flux in playa lakes in grassland and cropland basins, southern high plains of Texas. *Texas Water Journal*, 7(1), 25–39.
- Gibbs, J. P. (2000). Wetland loss and biodiversity conservation. *Conservation Biology*, 14(1), 314–317.
- Gorelick, N., Hancher, M., Dixon, M., Ilyushchenko, S., Thau, D., & Moore, R. (2017). Google earth engine: Planetary-scale geospatial analysis for everyone. *Remote Sensing of Environment*, 202, 18–27.
- Han, X., Chen, X., & Feng, L. (2015). Four decades of winter wetland changes in poyang lake based on landsat observations between 1973 and 2013. Remote Sensing of Environment, 156, 426–437.
- Han-Qiu, X. (2005). A study on information extraction of water body with the modified normalized difference water index (MNDWI). *Journal of Remote Sensing*, 5, 589–595.
- Hanski, I., & Ovaskainen, O. (2000). The metapopulation capacity of a fragmented landscape. *Nature*, 404(6779), 755–758.
- Hondula, K. L., DeVries, B., Jones, C. N., & Palmer, M. A. (2021). Effects of using high resolution satellite-based inundation time series to estimate methane fluxes from forested wetlands. *Geophysical Research Letters*, 48(6), e2021GL092556.
- Huang, C., Peng, Y., Lang, M., Yeo, I.-Y., & McCarty, G. (2014). Wetland inundation mapping and change monitoring using landsat and airborne lidar data. Remote Sensing of Environment, 141, 231–242.
- Huang, H., Chen, Y., Clinton, N., Wang, J., Wang, X., Liu, C., Gong, P., Yang, J., Bai, Y., Zheng, Y., & Zhu, Z. (2017). Mapping major land cover dynamics in Beijing using all landsat images in google earth engine. *Remote Sensing of Environment*, 202, 166–176.
- Huang, S., Young, C. J., Abdul-Aziz, O. I., Dahal, D., Feng, M., & Liu, S. (2013). Simulating the water budget of a prairie potholes complex from lidar and hydro logical models in North Dakota, USA. *Hydrological Sciences Journal*, 58(7), 1434–1444.
- Johnson, W. C., Werner, B., Guntenspergen, G. R., Voldseth, R. A., Millett, B., Naugle, D. E., Tulbure, M., Carroll, R., Tracy, J., & Olawsky, C. (2010). Prairie wetland complexes as landscape functional units in a changing climate. *Bioscience*, 60(2), 128–140.
- Jones, C. N., Evenson, G. R., McLaughlin, D. L., Vanderhoof, M. K., Lang, M. W., McCarty, G. W., Golden, H. E., Lane, C. R., & Alexander, L. C. (2018). Estimating restorable wetland water storage at landscape scales. *Hydrological Processes*, 32(2), 305–313.
- Kaplan, G., & Avdan, U. (2017). Mapping and monitoring wetlands using sentinel-2 satellite imagery. ISPRS Annals of Photogrammetry, Remote Sensing & Spatial Information Sciences, 4/W4, 271–277.
- Kayastha, N., Thomas, V., Galbraith, J., & Banskota, A. (2012). Monitoring wet land change using inter-annual landsat time-series data. Wetlands, 32(6), 1149–1162.
- Keddy, P. A. (2010). Wetland ecology: Principles and conservation. Cambridge University Press.
- LaBaugh, J. W. (1986). Wetland ecosystem studies from a hydrologic perspective 1. JAWRA Journal of the American Water Resources Association, 22(1), 1–10.
- Lane, C. R., & D'Amico, E. (2016). Identification of putative geographically isolated wetlands of the conterminous United States. JAWRA Journal of the American Water Resources Association, 52(3), 705–722.
- Lee, S., Yeo, I.-Y., Lang, M., Sadeghi, A., McCarty, G., Moglen, G., & Evenson, G. (2018). Assessing the cumulative impacts of geographically isolated wetlands on watershed hydrology using the swat model coupled with improved wetland modules. *Journal of Environmental Management*, 223, 37–48.
- Leibowitz, S. G. (2003). Isolated wetlands and their functions: An ecological perspective. *Wetlands*, 23(3), 517–531.
- Levy, M., Lopes, A., Cohn, A., Larsen, L., & Thompson, S. (2018). Land use change increases stream flow across the arc of deforestation in Brazil. Geophysical Research Letters, 45(8), 3520–3530.

- Liu, G., & Schwartz, F. W. (2011). An integrated observational and modelbased analysis of the hydrologic response of prairie pothole systems to variability in climate. Water Resources Research, 47(2), W02504. https://doi.org/10.1029/2010WR009084
- Maleki, S., Soffianian, A., Koupaei, S. S., Saatchi, S., & Pourmanafi, S. (2018). Application of remote sensing in monitoring unsustainable wetlands: Case study hamun wetland. *Journal of the Indian Society of Remote Sensing*, 46(11), 1871–1879.
- Mao, D., Wang, Z., Du, B., Li, L., Tian, Y., Jia, M., Zeng, Y., Song, K., Jiang, M., & Wang, Y. (2020). National wetland mapping in China: A new product resulting from object-based and hierarchical classification of landsat 8 oli images. ISPRS Journal of Photogrammetry and Remote Sensing, 164, 11–25.
- McKenna, O. P., Mushet, D. M., Rosenberry, D. O., & LaBaugh, J. W. (2017). Evidence for a climate-induced ecohydrological state shift in wetland ecosystems of the southern prairie pothole region. *Climatic Change*, 145(3), 273–287.
- McLaughlin, D. L., Kaplan, D. A., & Cohen, M. J. (2014). A significant nexus: Geographically isolated wetlands inuence landscape hydrology. Water Resources Research, 50(9), 7153-7166.
- Mekis, É., & Brown, R. (2010). Derivation of an adjustment factor map for the estimation of the water equivalent of snowfall from ruler measurements in Canada. Atmosphere-Ocean, 48(4), 284–293.
- Mullen, C., Penny, G., & Müller, M. F. (2021). A simple cloud-filling approach for remote sensing water cover assessments. Hydrology and Earth System Sciences, 25(5), 2373–2386.
- Müller, M. F., & Levy, M. C. (2019). Complementary vantage points: Integrating hydrology and economics for sociohydrologic knowledge generation. Water Resources Research, 55(4), 2549–2571.
- Müller, M. F., Yoon, J., Gorelick, S. M., Avisse, N., & Tilmant, A. (2016). Impact of the Syrian refugee crisis on land use and transboundary freshwater resources. *Proceedings of the National Academy of Sciences*, 113(52), 14932–14937.
- Muro, J., Canty, M., Conradsen, K., Hüttich, C., Nielsen, A. A., Skriver, H., Florian, R., Strauch, A., Thonfeld, F., & Menz, G. (2016). Short-term change detection in wetlands using sentinel-1 time series. *Remote Sensing*, 8(10), 795.
- Mushet, D. M., Rosenberry, D. O., Euliss N. H. Jr., & Solensky, M. J. (2016). Cottonwood lake study area-water surface elevations.
- Mushet, D. M., & Solensky, M. (2018). Cottonwood lake study area-amphibians. US Geological Survey data release. https://doi.org/10.5066/F7X9297Q
- Papa, F., Prigent, C., Durand, F., & Rossow, W. B. (2006). Wetland dynamics using a suite of satellite observations: A case study of application and evaluation for the indian subcontinent. *Geophysical Research Letters*, 33(8), L08401. https://doi.org/10.1029/2006GL025767
- Penny, G., Dar, Z. A., & Müller, M. F. (2022). Climatic and anthropogenic drivers of a drying Himalayan river. Hydrology and Earth System Sciences, 26(2), 375–395.
- Pérez Valentín, J. M., & Müller, M. F. (2020). Impact of hurricane maria on beach erosion in Puerto Rico: Remote sensing and causal inference. *Geophysical Research Letters*, 47(6), e2020GL087306.
- Reeves, C. C., & Reeves, J. A. (1996). The Ogallala aquifer of the southern high plains: Geology. Estacado Books.
- Rinaldo, A., & Rodriguez-Iturbe, I. (2022). *Ecohydrology 2.0* (pp. 1–26). Rendiconti Lincei. Scienze Fisiche e Naturali.
- Sader, S. A., Ahl, D., & Liou, W.-S. (1995). Accuracy of landsat-tm and gis rule based methods for forest wetland classification in maine. *Remote Sensing of Environment*, 53(3), 133–144.
- Schwatke, C., Scherer, D., & Dettmering, D. (2019). Automated extraction of consistent time-variable water surfaces of lakes and reservoirs based on landsat and sentinel-2. *Remote Sensing*, 11(9), 1010.
- Semlitsch, R. D., & Bodie, J. R. (1998). Are small, isolated wetlands expendable? *Conservation Biology*, 12(5), 1129–1133.

- Shaw, D. A., Pietroniro, A., & Martz, L. (2013). Topographic analysis for the prairie pothole region of western Canada. *Hydrological Processes*, 27(22), 3105–3114.
- Thompson, D. B., Reed, A., & Rainwater, K. (1994). Calibration of storm for modeling surface runoff to playa lakes at the pantex plant. In *Proceedings of the playa basin symposium* (pp. 153–157).
- Todhunter, P. E. (2016). Mean hydroclimatic and hydrological conditions during two climatic modes in the devils lake basin, North Dakota (USA). Lakes & Reservoirs: Research & Management, 21(4), 338–350.
- Van Meter, K. J., & Basu, N. B. (2015). Signatures of human impact: Size distributions and spatial organization of wetlands in the prairie pothole landscape. *Ecological Applications*, 25(2), 451–465.
- Walpole, M., & Davidson, N. (2018). Stop draining the swamp: it's time to tackle wetland loss. *Oryx*, *52*(4), 595–596.
- Werner, E. E., Skelly, D. K., Relyea, R. A., & Yurewicz, K. L. (2007). Amphibian species richness across environmental gradients. *Oikos*, 116(10), 1697–1712.
- Winter, T. C., & LaBaugh, J. W. (2003). Hydrologic considerations in defining isolated wetlands. *Wetlands*, 23(3), 532–540.
- Winter, T. C., & Rosenberry, D. O. (1995). The interaction of ground water with prairie pothole wetlands in the cottonwood lake area, East-Central North Dakota, 1979–1990. *Wetlands*, 15(3), 193–211.

- Wu, Q., Lane, C. R., Li, X., Zhao, K., Zhou, Y., Clinton, N., DeVries, B., Golden, H., & Lang, M. W. (2019). Integrating lidar data and multi-temporal aerial imagery to map wetland inundation dynamics using google earth engine. *Remote Sensing of Environment*, 228, 1–13.
- Zhao, G., & Gao, H. (2018). Automatic correction of contaminated images for assessment of reservoir surface area dynamics. *Geophysical Research Letters*, 45(12), 6092–6099.

#### SUPPORTING INFORMATION

Additional supporting information can be found online in the Supporting Information section at the end of this article.

How to cite this article: Mullen, C., Bertassello, L. E., Rao, P. S. C., & Müller, M. F. (2022). From wetlands to wetlandscapes: Remote sensing calibration of process-based hydrological models in heterogeneous landscapes. *Hydrological Processes*, 36(11), e14739. <a href="https://doi.org/10.1002/hyp.14739">https://doi.org/10.1002/hyp.14739</a>